Section 1

Direct collider search of WIMPs

In this section, we review the production of TeV-scale WIMPs and search for their signals using collider experiments. In particular, we will summarize the current bounds for WIMPs obtained at the large hadron collider (LHC) and prospects at the future planned 100 TeV colliders such as the hadron option of the future circular collider (FCC-hh) [?] and the super proton-proton collider (SPPC) [?, ?]. In Sec. 1.1, we discuss the dominant production processes of WIMPs at a hadron collider. In Sec. 1.2 and Sec. 1.3, we review two different methods for the signal identification, the disappearing track search and the mono-jet search, and summarize the current and future bounds.

1.1 WIMP production

There are two relevant processes both of which significantly contribute to the production cross section of WIMPs considered here. The pair production via electroweak interaction is a universal process that can be considered for any particle with a non-zero electroweak charge. The decay of colored particles may also be efficient particularly for the MSSM. In this subsection, we will review these two in order.

Pair production via electroweak interaction

Since all the WIMPs of our interest possess non-zero $SU(2)_L$ and/or $U(1)_Y$ charges, they can be directly produced via electroweak interaction at the hadron collider as shown in
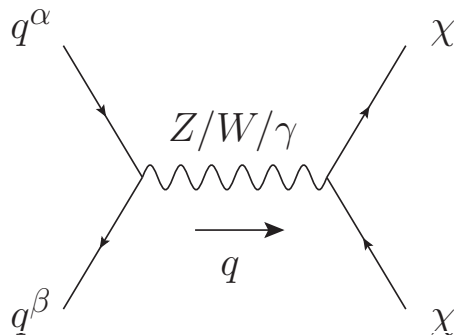

Figure 1: WIMP pair production process at the hadron collider.

Fig. 1.[♮1] In the figure, q^α and q^β denote the partons (namely, one of the quarks)[♮2] of the incident protons relevant for the process, while χ denotes the WIMP and q is the momentum transfer. Assuming the WIMP to be a $SU(2)_L$ n-plet with $U(1)_Y$ charge Y and the mass m_χ, this process is well described by the effective lagrangian[♮3]

$$\mathcal{L} = \mathcal{L}_{\mathrm{SM}} + (D^\mu \chi)^\dagger (D_\mu \chi) - m_\chi^2 \chi^\dagger \chi \qquad \text{(complex scalar)}, \qquad (1.1)$$

$$\mathcal{L} = \mathcal{L}_{\mathrm{SM}} + \bar{\chi}(i\slashed{D} - m_\chi)\chi \qquad \text{(Dirac fermion)}, \qquad (1.2)$$

with $\mathcal{L}_{\mathrm{SM}}$ being the SM lagrangian, while the covariant derivative is given by

$$D_\mu \equiv \partial_\mu - ig_2 \slashed{W}^a T_n^a - ig_1 Y \slashed{B}, \qquad (1.3)$$

where T_n^a ($a = 1, 2, 3$) are n-dimensional representation matrices of $SU(2)_L$. Note that when χ is a real scalar (Majorana fermion) with $Y = 0$, the terms with χ in Eq. (1.1) (Eq. (1.2)) should be divided by two.

For the calculation, we neglect the effect of the electroweak symmetry breaking, which is valid because we are interested in the high-energy collision with the parton-level center-of-mass (CM) energy $\sqrt{s'} \equiv \sqrt{q^2} \gtrsim$ TeV. Then, we consider the process in the CM frame and estimate the parton-level differential cross section as

$$\left.\frac{d\sigma_{\alpha\beta}}{d\Omega}\right|_{\sqrt{s'},\mathrm{CM}} = \frac{C_{\alpha\beta}}{8s'}\left(1 - \frac{4m_\chi^2}{s'}\right)^{3/2}\sin^2\theta_{\mathrm{CM}} \qquad \text{(complex scalar)} \quad (1.4)$$

$$\left.\frac{d\sigma_{\alpha\beta}}{d\Omega}\right|_{\sqrt{s'},\mathrm{CM}} = \frac{C_{\alpha\beta}}{4s'}\sqrt{1 - \frac{4m_\chi^2}{s'}}\left[1 + \frac{4m_\chi^2}{s'} + \left(1 - \frac{4m_\chi^2}{s'}\right)\cos^2\theta_{\mathrm{CM}}\right] \quad \text{(Dirac fermion)}, \quad (1.5)$$

where θ_{CM} is the angle between the momentum of the initial parton q^α and that of a final state WIMP. These expressions are valid only when the CM energy exceeds the production threshold, $\sqrt{s'} > 2m_\chi$. Note also that these expressions represent inclusive cross sections, *i.e.*, the total cross section for the production of all components of the WIMP multiplet χ.

[♮1]All the Feynman diagrams in this thesis are drawn with the public code `JaxoDraw-2.1` [?], which is a graphical user interface that allows users to draw Feynman diagrams intuitively and export them in the `eps` format with the help of the (modification of) `axodraw` style file for LaTeX [?]. Under the environment of macOS Mojave, it apparently fails to start, but one can still execute it by looking inside the application and start the Java executable file `jaxodraw-2.1-0.jar` directly. We would like to thank the authors for providing the best tools to write the thesis with.

[♮2]When we take account of the next-to-leading order QCD effect, gluon may also be one of the initial partons.

[♮3]In this subsection, we neglect the small mass splitting among different components in the multiplet χ described in Sec. **??**. This approximation is valid since the mass splitting is by far smaller than m_χ and has only a tiny effect on the production process.

The coefficient $C_{\alpha\beta}$ consists of contributions from $U(1)_Y$ and $SU(2)_L$ gauge bosons,[♮4]

$$C_{\alpha\beta} = c_{1\alpha\beta}Y^2\alpha_1^2 + c_{2\alpha\beta}I(n)\alpha_2^2, \tag{1.6}$$

with $I(n)$ being the Dynkin index for the n-dimensional representation given by

$$I(n) \equiv \frac{n^3 - n}{12}, \tag{1.7}$$

which is normalized so that $I(2) = 1/2$. The explicit form of $c_{1\alpha\beta}$ and $c_{2\alpha\beta}$, which are sizes of the couplings between partons of our choice and gauge bosons, can be expressed using the $U(1)_Y$ charge Y_α of the parton q^α and the reducible representation matrices of $SU(2)_L$ in the parton basis $T^a_{\alpha\beta}$ as

$$c_{1\alpha\beta} = Y_\alpha^2\delta_{\alpha\beta}, \tag{1.8}$$

$$c_{2\alpha\beta} = \sum_a \left|T^a_{\alpha\beta}\right|^2. \tag{1.9}$$

Recalling that $\alpha_1 < \alpha_2$ and that we often consider the WIMPs with large n and moderate Y, the WIMP production cross section grows as n^3 for larger multiplets according to the group theoretical factor (1.7).

In reality, the initial state of the hadron collider is not the individual partons but two protons. To obtain the cross section for the two-proton initial state, we rely on the parton distribution function (PDF), which expresses the fraction of the partons with some given momentum in each accelerated proton (see for example [?, ?]). Let $f_\alpha(x)$ $(0 < x < 1)$ be the PDF for a given parton q^α inside a proton with momentum p^μ. $f_\alpha(x)$ can be interpreted as a probability distribution to find the parton q^α with momentum xp^μ, so we have a relationship

$$\sum_\alpha \int_0^1 dx\, x f_\alpha(x) = 1, \tag{1.10}$$

associated with the total momentum conservation, and

$$\int_0^1 dx\, [f_d(x) - f_{\bar{d}}(x)] = 1, \tag{1.11}$$

$$\int_0^1 dx\, [f_u(x) - f_{\bar{u}}(x)] = 2, \tag{1.12}$$

from the composition of the proton. Using the PDF, the cross section of the process of interest at the hadron collider is evaluated as

$$\frac{d\sigma}{d\sqrt{s'}d\Omega} = \sum_{\alpha,\beta} \int_0^1 dx_1 dx_2\, f_\alpha(x_1)f_\beta(x_2)\delta\left(s' - sx_1x_2\right) \frac{d\sigma_{\alpha\beta}}{d\Omega}\bigg|_{\sqrt{s'},\text{lab}}, \tag{1.13}$$

[♮4]There is no contribution from the interference term between $U(1)_Y$ and $SU(2)_L$ contributions, since it is proportional to $\text{Tr}(T_n^a) = 0$.

Figure 2: Example of NLO QCD contributions to the WIMP pair production process.

where $\sqrt{s}$ is the CM energy of the proton-proton collision. Note that $d\sigma_{\alpha\beta}/d\Omega\,|_{\sqrt{s'},\text{lab}}$ in the integrand, which is a differential cross section in the laboratory, is a function of x_1 and x_2, which is obtained by applying the appropriate Lorentz transformation to $d\sigma_{\alpha\beta}/d\Omega\,|_{\sqrt{s'},\text{CM}}$. Precisely speaking, the PDF has an energy scale dependence which is determined by the Dokshitzer-Gribov-Lipatov-Altarelli-Parisi (DGLAP) equation [?, ?, ?, ?]. Thus, the PDF is a function of the form $f(x, \mu_F)$, where μ_F is the analog of the renormalization scale for the PDF often called the factorization scale.

Hadron colliders have several more features related to the strong interaction of quantum chromodynamics (QCD). Firstly, the next-to-leading order (NLO) QCD contribution to each process is not necessarily negligible. For the WIMP pair production, the real and virtual emission of a gluon shown in the left and right panels of Fig. 2, respectively, give the NLO QCD contributions. In particular, when the large transverse momentum is important for the phenomenology of our concern, such as the case in Sec. 1.2, the real emission of a gluon with a sizable transverse momentum significantly modifies the cross section relevant for the analysis. Also, an additional real emission may be required to trigger the event, in particular when the other products are invisible for detectors like in Sec. 1.3. Secondly, all the colored particles in the initial, intermediate, and final states should be accompanied by numbers of soft emissions of gluons, which can be treated by the semi-classical approximation called the parton shower. In practice, there is a difficulty caused by the partial overlap of the gluon phase space between the one-gluon emission cross section calculated as an NLO QCD effect and the same calculated by the parton shower. To avoid the overlap, we often perform the matching procedure, in which we set some merging energy scale by hand and include the contribution to the cross section with gluon energy above (below) the scale only from the NLO QCD (parton shower) calculation. Finally, the colored particles in the final states should eventually be confined, which is called the hadronization, and observed as some energetic and collimated sprays of hadrons, which as a whole is called a jet.

In the following, we perform the numerical calculation, taking account of all the above complexities. For this purpose, we make use of the Monte Carlo generator `MadGraph5`

WIMP name	Higgsino	Wino	5-plet Majorana fermion
σ_{LO} [fb]	15	85	423
σ_{NLO} [fb]	17	93	461
K-factor	1.15	1.09	1.09

Table 1:   Table of pair production cross sections of several types of WIMPs. The CM energy $\sqrt{s} = 100\,\mathrm{TeV}$ is assumed and WIMP masses are set to be $1\,\mathrm{TeV}$.

Wino mass [TeV]	1.0	1.5	2.0	2.9
σ_{LO} [fb]	85	19	6.1	1.3
σ_{NLO} [fb]	93	21	6.8	1.5
K-factor	1.09	1.11	1.11	1.15

Table 2:   Table of pair production cross sections of Wino with several choice of masses. The CM energy $\sqrt{s} = 100\,\mathrm{TeV}$ is assumed.

aMC@NLO (v2.6.3.2) [?, ?] with the successive use of Pythia8 [?] for the parton shower, hadronization, and matching and Delphes (v3.4.1) [?] for the detector simulation, including the definition of jets as observed objects. We use the MLM-style matching [?] with the merging scale of $67.5\,\mathrm{GeV}$ and NNPDF2.3QED with $\alpha_3(M_Z) = 0.118$ [?] as a canonical set of PDFs. For the renormalization and factorization scales, we adopt the default values of MadGraph5 aMC@NLO, *i.e.*, the central m_T^2 scale after k_T-clustering of the event. The one-loop level contributions such as the right panel of Fig. 2 can be taken into account by using a properly prepared model file and the [QCD] option of MadGraph5. However, just for simplicity of the analysis, we generate the tree-level pair production process with up to one jet.[♮5]

In Table 1, we list the production cross sections of various WIMPs via a weak gauge boson exchange at a $\sqrt{s} = 100\,\mathrm{TeV}$ hadron collider.[♮6] As for the WIMP mass, we use the common value $m = 1\,\mathrm{TeV}$ to compare the cross sections among a different choice of quantum numbers. σ_{LO} and σ_{NLO} denote the production cross sections without and with the NLO QCD correction, respectively, while the last line is the so-called K-factor defined as $\sigma_{\mathrm{NLO}}/\sigma_{\mathrm{LO}}$. From the table, by comparing the results for the triplet (*i.e.* Wino) and 5-plet Majorana fermions, we can roughly see the correct dependence of the cross section on the $SU(2)_L$ charge $\sigma \propto n^3$.

[♮5]In spite of the lack of the one-loop contributions, this procedure is free from the infrared divergence since the matrix element with an additional jet is considered only when the jet energy scale is larger than the merging scale.

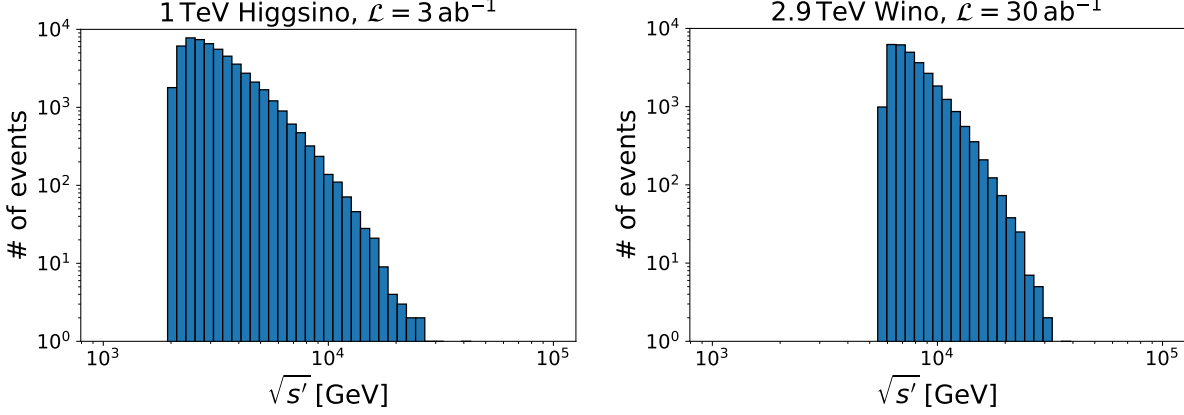[♮6]See Appendix ?? for the implementation of the MDM model in the collider simulation procedure.

Figure 3: Histogram of the $\sqrt{s'}$ distribution for $\sqrt{s} = 100\,\text{TeV}$. *Left:* Production of $1\,\text{TeV}$ Higgsino at $\mathcal{L} = 3\,\text{ab}^{-1}$. *Right:* Production of $2.9\,\text{TeV}$ Wino at $\mathcal{L} = 30\,\text{ab}^{-1}$.

In Table 2, we also show the mass dependence of the Wino pair production cross section. For heavier mass, a wider range of $\sqrt{s'}$ is below the production threshold $2m_\chi$ or accompanied with a small suppression factor $\left(1 - 4m_\chi^2/s'\right)^{1/2}$ as shown in Eq. (1.5), and the cross section becomes significantly smaller. However, values in the tables still show that plenty of well-motivated WIMP DM candidates, such as $1\,\text{TeV}$ Higgsino and $2.9\,\text{TeV}$ Wino, are produced at, for example, the $30\,\text{ab}^{-1}$ option of the FCC-hh.

In Fig. 3, we show the $\sqrt{s'}$ distribution for the pair production process at a $\sqrt{s} = 100\,\text{TeV}$ collider. Left and right figures correspond to the production of $m_\chi = 1\,\text{TeV}$ Higgsino at the integrated luminosity $\mathcal{L} = 3\,\text{ab}^{-1}$ and of $m_\chi = 3\,\text{TeV}$ Wino at $\mathcal{L} = 30\,\text{ab}^{-1}$, respectively. At around $\sqrt{s'} \sim 2m_\chi$, we clearly see the production threshold and the suppression effect $\sigma \propto (1 - 4m_\chi^2/s')^{1/2}$. On the other hand, when $\sqrt{s'}$ becomes much larger than $2m_\chi$, the cross section rapidly decreases because of both the scaling of the parton-level cross section $\sigma \propto (\sqrt{s'})^{-3}$ as in Eq. (1.5) and the smaller values of the PDF. Note that these properties are universal among several processes, including one of the contributions to the gluino pair production process through the s-channel gluon exchange discussed in the next subsection and the lepton pair production via an electroweak gauge boson that is the main topics of Sec. **??**.

Decay of colored particles

In hadron colliders, a particle with the color charge has far more chance to be produced than a non-colored particle with the same mass. When we consider the split SUSY or the anomaly mediation model reviewed in Sec. **??**, gluino tends to be relatively light, whose decay produces WIMPs. Without fine-tuning of Higgsino and gaugino masses, gluino lifetime is

gluino mass [TeV]	6.0	7.0	8.0
$\sigma(pp \to \tilde{g}\tilde{g})$ [fb]	7.9	2.7	1.0

Table 3:   Gluino pair production cross section at $\sqrt{s} = 100\,\mathrm{TeV}$ at the leading order of α_s taken from [?].

sufficiently short and only its decay products are observed by the detectors. Since all the SUSY particles finally decay into the LSP as described in Sec. **??**, the gluino production cross section can effectively be counted as the production cross section of WIMPs in these models.

Keeping the R-parity conservation in our mind, the dominant process accompanied by gluinos in these models is the gluino pair production. In Table 3, we summarize the gluino pair production cross section evaluated at the leading order of α_s for simplicity for various gluino masses at $\sqrt{s} = 100\,\mathrm{TeV}$, taken from [?]. The values in the table show that the gluino pair production process, depending on masses of gluino and WIMP, may give a much larger cross section for the WIMP production than the purely electroweak processes described above. We will mainly focus on, however, the electroweak pair production process below, in case gluino is out of the reach at 100 TeV colliders.

1.2   Disappearing track search

In the last section, we have checked the possibility that a large number of WIMPs are produced at hadron colliders. On the other hand, the detection of produced WIMPs is not a straightforward task, because there are huge background events with many charged and/or colored particles. To reduce the background events and obtain the best possible reach for WIMPs, we consider several methods using typical properties for the WIMP signals, one of which is the disappearing track signal described here.

As mentioned in Sec. **??**, the spontaneous breaking of the electroweak symmetry leads to the mass splitting among an $SU(2)_L$ multiplet, leaving the neutral component as the lightest one. As a result, the charged components of a multiplet, if produced, eventually decay into the neutral component. However, the mass splitting is so small in many cases that the typical flight length of the charged components is comparable to the detector size. Such long-lived charged particles, which travel for a few cm and then decay into an invisible counterpart, can be detected as charged tracks disappearing in the middle. They are very characteristic signals and can be used as an efficient discriminator between the SM background and the WIMP signals. In this section, we will study what we have summarized above in more detail.

Lifetime of charged components

The small mass splitting among a WIMP multiplet allows the heavier charged component to decay into the neutral component and SM particles via an off-shell W boson. Depending on the size of the relevant mass difference Δm_χ, several channels contribute to the decay [**?**]. For tiny $\Delta m_\chi < m_\pi$ with m_π being the charged pion mass, $\chi^\pm \to \ell^\pm \nu_\ell \chi^0$ ($\ell = e, \mu$) are the unique decay modes. Once Δm_χ exceeds m_π, the mode $\chi^\pm \to \pi^\pm \chi^0$ opens up and becomes the dominant one. After $\Delta m_\chi \gtrsim 1\,\mathrm{GeV}$, final states with two and three pions start to give a sizable contribution, and the total decay rate asymptotes to that for $\chi^\pm \to q'\bar{q}\chi^0$. For a larger mass splitting, the mode $\chi^\pm \to \tau^\pm \nu_\tau \chi^0$ may also be allowed. As a whole, these decay modes determine the lifetime of a charged component of a WIMP, which is typically long enough to be probed by experiments thanks to the small mass difference.

Let τ be the lifetime of the (singly) charged component of a WIMP, defined using the total decay rate Γ as $\tau \equiv 1/\Gamma$. Taking into account that a WIMP, if produced at colliders with sufficiently high energy, has a velocity comparable to the speed of light c, $c\tau$ expresses a rough estimation of its flight length inside detectors. For Higgsino with $m_\pi < \Delta m_\chi \lesssim 1\,\mathrm{GeV}$,[♮7] we can estimate [**?**,**?**]

Disappering track signal

Once a long-lived charged component of WIMP is produced, it is detected by the trackers installed in the innermost part of the detectors for the case of ATLAS and CMS collaborations at the LHC. For example, in the ATLAS setup, several tracking detectors are equipped cylindrically around the beamline from the radius $r = 3\,\mathrm{cm}$ to $108\,\mathrm{cm}$. The pixel detector spans the radius from $3\,\mathrm{cm}$ to $12\,\mathrm{cm}$, the strip semiconductor tracker (SCT) from $30\,\mathrm{cm}$ to $52\,\mathrm{cm}$, and the transition radiation tracker from $56\,\mathrm{cm}$ to $108\,\mathrm{cm}$. In particular, the pixel detector is the most important for our discussion, which is composed of four layers, with the innermost one being the recently equipped so-called the insertable B-layer [**?**,**?**,**?**]. To detect the charged track signal of a long-lived WIMP with the typical flight length of $\mathcal{O}(1)\,\mathrm{cm}$, they require the hit at every layer of the pixel detector and apply the SCT veto to search for the track signal disappearing in between $12\,\mathrm{cm} < r < 30\,\mathrm{cm}$. As for the fake events within the SM, the SCT veto denies the possibility for a stable SM particle to mimic the signal. However, there are two important sources of the fake track generated by hadrons/electrons and the so-called pile-up.

The first possibility with hadrons/electrons is a physical background caused by the interaction of hadrons with detector material or by the hard photon emission of electrons. After

---

[♮7]We are not interested in Higgsino with $\Delta m_\chi \gtrsim 1\,\mathrm{GeV}$ here since the corresponding flight length will be much shorter than $\mathcal{O}(1)\,\mathrm{cm}$, which is the scale of the detectors.

these interactions, the orbit of a hadron/electron is bent and, if this secondary interaction occurs in between $12\,\mathrm{cm} < r < 30\,\mathrm{cm}$, two tracks in the pixel detector and the SCT are not identified with each other. As a result, the first track in the pixel detector seems to disappear in the middle, which mimics the true WIMP signals. In the LHC, this type of background dominates and generates $\mathcal{O}(10\text{–}100)$ fake events for $\sqrt{s} = 13\,\mathrm{TeV}$, $\mathcal{L} = 36.1\,\mathrm{fb}^{-1}$ (see Fig. 7 of [?]).

On the other hand, for future hadron colliders, the second possibility of the fake track from the pile-up may be more important. In hadron colliders, a bunch of protons is accelerated at the same time and two bunches "collide" with each other with some given frequency. Since there are many protons inside a bunch, typically more than one collisions of two protons occur for each bunch crossing. The average number of collisions per bunch crossing is often denoted as $\langle \mu \rangle$ and the values of $\langle \mu \rangle \sim 20$, 80, and 200 are expected for LHC Run-2, Run-3, and HL-LHC. With this large number of collisions, there are a lot of collision products detected almost at the same time, which makes the signal significantly messy. Then, among a huge number of hits on tracking detectors, several of them occasionally form a straight line in position and time, which is sometimes called the fake track. Since this track is only a fake, it can easily pass the SCT veto and mimic the disappearing track signal of WIMPs. In the real experiment, the rate for fake track reduces as we require more hits on trackers. See the results reviewed below for a concrete estimation of the fake track rate at the FCC-hh.

From now on, we estimate how many events are expected at the FCC-hh. Recalling that the detectors are installed in a cylindrical geometry, the transverse distance d_T of the charged WIMP flight measured from the beamline plays an important role. We can estimate the probability for d_T to be larger than d as

$$P(d_T > d) = \exp\left(-\frac{d}{\beta\gamma c\tau \sin\theta}\right), \qquad (1.14)$$

where β is the WIMP velocity, $\gamma \equiv (1 - \beta^2)^{-1/2}$, and θ is the angle between the WIMP momentum and the beamline. One of the implications of the above expression is that WIMPs with large transverse momentum have a larger possibility to reach outer layers of the pixel detector. This enlarges the importance of considering the NLO (and higher-order) QCD processes with real emissions for the pair production. Due to the hard emission of the gluon, the produced pair of WIMPs recoil in the opposite direction, and WIMPs tend to have larger transverse momentum than the case without gluon emission. It can be directly checked that, for $\sqrt{s} = 100\,\mathrm{TeV}$, even the two-gluon emission process possesses non-negligible contribution to the simulation of the disappearing track search for WIMPs.

In Fig. 4, we show the distribution of $P(d_T > 15\,\mathrm{cm})$, which is motivated by the FCC-hh detector setup assumed below, for the 2.9 TeV Wino, $\sqrt{s} = 100\,\mathrm{TeV}$, and $\mathcal{L} = 30\,\mathrm{ab}^{-1}$. The blue and orange histograms show the distributions without and with the cut on the
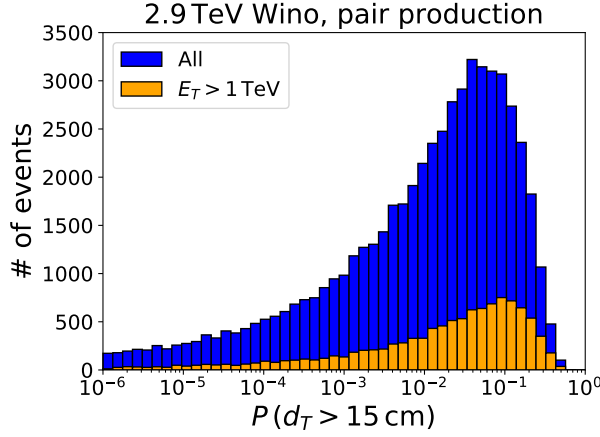
Figure 4:   Distribution of the survival probability $P(d_T > 15\,\text{cm})$ for 2.9 TeV Wino. The pair prodction process at $\sqrt{s} = 100\,\text{TeV}$ and $\mathcal{L} = 30\,\text{ab}^{-1}$ is assumed.

missing transverse momentum $\not{E}_T > 1\,\text{TeV}$, respectively, which has been revealed to be efficient to reduce the number of backgrounds [**?**]. Here, we only consider the WIMP pair production process with up to one gluon emission as an example. Note that $\tau \simeq 5.8\,\text{cm}$ and $\exp(-15\,\text{cm}/\tau) \sim 7.5 \times 10^{-2}$ for this setup. We can see that the effect of the large Lorentz boost $\beta\gamma \gg 1$ pushes the probability to $P \gtrsim \mathcal{O}(10^{-1})$ for some Winos, while the angular distribution of Winos makes a wide tail of the distribution at $P \lesssim \mathcal{O}(10^{-2})$ when $\sin\theta \sim 0$. By summing the shown probabilities for all produced Winos, we can obtain the expectation value N_{15} for the number of Winos with $d_T > 15\,\text{cm}$. We find $N_{15} \sim 2700$ (700) with (without) the $\not{E}_T$ cut, to which a lot of Winos with $P \gtrsim \mathcal{O}(10^{-1})$ significantly contribute. Thus, we infer that we can detect the Wino signal if we can suppress the number of background events to $\lesssim \mathcal{O}(10^5)$. In the next subsection, we will see that this may be the case for the FCC-hh and the parameter space for the Wino DM candidate can fully be covered.

In Fig. 5, we show the distribution of the Wino velocity β for the same process. The blue and orange histograms show the distributions without and with the $\not{E}_T$ cut, respectively, while the green one shows that with $\not{E}_T > 1\,\text{TeV}$ and $d_T > 15\,\text{cm}$, picked up randomly according to the survival probability Eq. (1.14). As already seen in Fig. 3, the CM energy of the two-Wino system distributes from a few to $\mathcal{O}(10)\,\text{TeV}$, and many Winos are highly boosted with $\beta \sim 1$. Since a charged Wino tends to survive for a longer distance when it is more accelerated, a non-negligible fraction of the boosted Winos with $\beta \gtrsim 0.6$ satisfies the requirement $d_T > 15\,\text{cm}$.
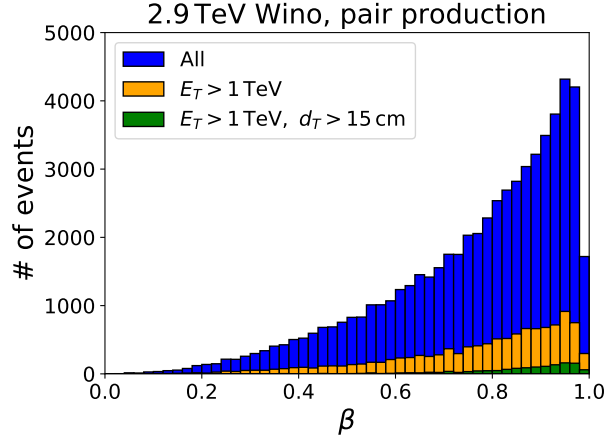
Figure 5:   Distribution of the Wino velocity β for 2.9 TeV Wino. The pair prodction process at $\sqrt{s} = 100\,\text{TeV}$ and $\mathcal{L} = 30\,\text{ab}^{-1}$ is assumed.

WIMP	pure Higgsino	Wino	5-plet fermion
Upper bound on m_χ	152 GeV	460 GeV	267 GeV

Table 4:   Current upper bounds for WIMP masses obtained from the disappearing track search. Results are taken from [**?**, **?**, **?**, **?**].

Current constraints and future prospects

So far, the disappearing track search is performed by both ATLAS [**?**] and CMS [**?**] collaborations. Below, we will focus particularly on the ATLAS collaboration and discuss current constraints.

In Fig. 6, we show the result of the disappearing track search taken from [**?**]. As for the production process, only the pair production via an electroweak gauge boson is considered. The yellow band shows the current constraint on the WIMP mass and lifetime plane and the left part of the band is already excluded. The sensitivity becomes weak when we consider $\tau \gtrsim 1\,\text{ns}$ or $c\tau \gtrsim 30\,\text{cm}$ due to the requirement of the SCT veto. In the figure, the lifetime of Wino as a function of its mass is also shown by the black dot-dashed line. It can be seen that the current constraint on Wino mass is $m_\chi \lesssim 460\,\text{GeV}$.

Using the lifetime evaluated in the previous subsection, we summarize the current status for several WIMPs in Table 4, which exhibits upper limits of $\mathcal{O}(100)\,\text{GeV}$. However, note that the bound for the Higgsino listed in the table neglects the mixing between Higgsino and gauginos. Actually, Δm_χ and thus τ are sensitive to the mixing, and an order estimation shows that the mixing lowers the lifetime to be $\tau \lesssim 0.01\,\text{ns}$ and spoils the bound for Higgsino when $M_1, M_2 \lesssim 100\,\text{TeV}$ without any non-trivial cancellation in Eq. (**??**). Note also that the
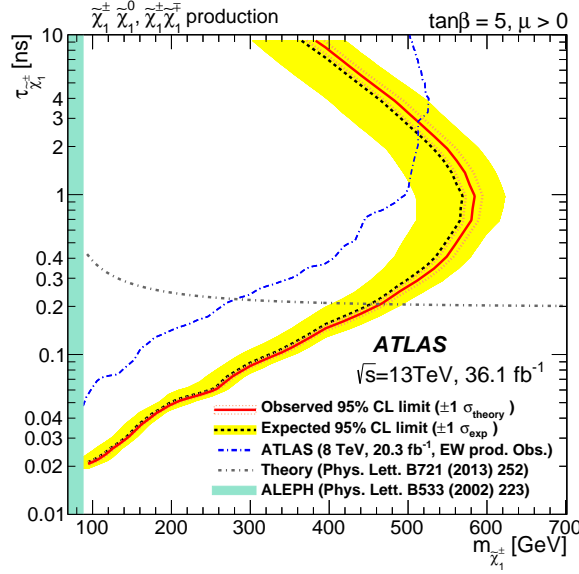
Figure 6:   Current status of the disappearing track search using the pair production process via an electroweak gauge boson. The figure is taken from [**?**].

Detector setup	pure Higgsino	Wino
$r_5 = 15\,\mathrm{cm}$	0.9–1.2 TeV	$> 4.0\,\mathrm{TeV}$
$r_5 = 27\,\mathrm{cm}$	$< 0.7\,\mathrm{TeV}$	2.9–4.0 TeV

Table 5:   Prospects of 5σ discovery reach of the disappearing track search at the FCC-hh with $\mathcal{L} = 30\,\mathrm{ab}^{-1}$ using the pair production process via an electroweak gauge boson. The results are based on [**?**].

bound for 5-plet fermion is weaker than that for Wino in spite of the much larger production cross section because of the smaller lifetime.

   The analysis of the disappearing track search at future hadron colliders is performed in [**?**, **?**]. Since the detector setup for future colliders such as the FCC-hh is undetermined yet, in [**?**], the authors assume several setups and compare the result. In each setup, five layers of the pixel detector are installed and the fifth layer position (which we call r_5) ranges from 15 cm to 27 cm.[♮8] For the background reduction, hits to all of the five layers are required. By varying the average number of pp interactions per bunch crossing from $\langle \mu \rangle = 200$ to 500, the fake background rate is estimated to range from 10^{-7} to 10^{-5}.

[♮8]For simplicity of the discussion, we just assume that the detectors outside the pixel detector are far apart from the beamline so that all the WIMPs decay before reaching them. Then, we can estimate the discovery reach by counting the number of WIMP signals that reach the fifth layer of the pixel detector.

In Table 5, we summarize the obtained 5σ discovery reach for pure Higgsino and Wino for two detector setups with the integrated luminosity $\mathcal{L} = 30\,\mathrm{ab}^{-1}$, again using the pair production process via an electroweak gauge boson. The uncertainty of the reach corresponds to the variation of $\langle\mu\rangle = 200$–500 and the uncertainty in soft QCD processes. Recalling the discussion in Sec. **??**, Table 5 shows that the FCC-hh can cover the whole region of the parameter space consistent with Wino DM $m_\chi \lesssim 2.9\,\mathrm{TeV}$. On the other hand, there is a sensitivity up to the mass of the thermal Higgsino DM $m_\chi \sim 1.1\,\mathrm{TeV}$ only when we adopt the most optimistic assumption, $i.e.$, the pure Higgsino with small Δm_χ searched for with $r_5 = 15\,\mathrm{cm}$. Thus, it is an important task to consider another way of search for Higgisno, in particular, a way that is unaffected by the mass splitting Δm_χ. The authors do not give any comment on the MDM search, but we can give some very rough estimates of the reach from Table 5. For example, considering the 5-plet fermion with $c\tau \sim 1.8\,\mathrm{cm}$, the size of the significance of the signal should be in between that for Higgsino and Wino assuming the same production cross section, while the cross section scales as n^3 as a function of the $SU(2)_L$ charge as we have seen so far. Thus, the reach for the 5-plet fermion should be a few TeV, which covers a non-negligible fraction of the parameter space viable as a DM candidate.

1.3   Mono-jet search

Another way of identifying the WIMP events is to look for the mono-jet events. The relevant process is shown in the left panel of Fig. 2; if the WIMP pair production occurs with an initial state radiation (ISR) jet but both of the WIMPs are unobserved by detectors, the unique object that is observed is the ISR jet. In the mono-jet search, we require this jet to be sufficiently hard and use it to trigger and tag the event as an event related to the new physics.

Since the event topology is astonishingly simple, there are a huge number of background events within the SM. The dominant background comes from the Z+jet production with Z decaying into two neutrinos. Besides, the W+jet production followed by the leptonic decay of the W-boson has a comparable contribution because the charged lepton in the final state may fall outside the detector coverage. Finally, a sub-dominant but non-negligible contribution to the background comes from the top pair production process and so on. These background events lead to the small signal-to-background ratio (S/B) of the $1\,\%$ level both within the current setup and the future prospect, which makes this method highly challenging.

Considering the small ratio S/B, the systematic errors may also shrink the discovery reach of WIMPs in this method. At worst, these errors should be as small as the $1\,\%$ level to obtain some meaningful results. However, this may be overcome by future endeavors both in the theory and experimental sides. For example, the theoretical and experimental values

systematic error σ_B	Higgsino	Wino
1%	$0.5\,\mathrm{TeV}$	$1\,\mathrm{TeV}$
2%	$0.2\,\mathrm{TeV}$	$0.5\,\mathrm{TeV}$

Table 6:   Prospects of 5σ discovery reach of the mono-jet search at the FCC-hh with $\mathcal{L} = 30\,\mathrm{ab}^{-1}$ using the pair production process via an electroweak gauge boson. The results are based on [?].

of the relevant cross sections are already controlled with high precision. In the theory side, the errors in the calculation are reduced to a few percent level by including the next-to-next-to-leading order QCD and the NLO electroweak effects and performing the next-to-leading logarithmic resummation of the electroweak Sudakov factors [?]. In the experimental side, the uncertainties on the estimation of the cross section of background events from the data are also at a few percent level [?]. These errors are expected to be reduced with the calculation of the higher order loop effects and the accumulation of more data.

The main focus of this method is on the short lifetime Higgsino since the other long-lived WIMPs will be more efficiently searched for by the disappearing track search. Unfortunately, due to the small ratio S/B, there is no constraint on the Higgsino from the mono-jet search so far [?]. As for the future prospects, we show the prospects of 5σ discovery reach for Higgsino and Wino taken from [?] in Table 6. To obtain the result, the authors introduce the parameter σ_B (σ_S) that expresses the unknown systematic uncertainty on the background (signal) and define the p-value as

$$p \equiv \frac{S}{\sqrt{B + (\sigma_B B)^2 + (\sigma_S S)^2}}, \tag{1.15}$$

where B and S are the number of background and signal events, respectively. The denominator combines the errors from the statistical fluctuation (the corresponding standard deviation equals $\sqrt{B}$), the systematic errors on the background ($\sigma_B B$), and those on the signal ($\sigma_S S$), assuming that all of the above are uncorrelated with each other. They fix $\sigma_S = 10\%$ and use two different choices $\sigma_B = 1\%$ and 2% as the table shows. The values on the table correspond to the WIMP masses that give $p = 5$.

From the table, we can see that the result highly depends on the choice of σ_B. In particular, it is important to suppress $\sigma_B \lesssim 1\%$ to obtain a strong discovery reach on Higgsino. Besides, it can be checked that the coverage of the Wino parameter space is much smaller than that of the disappearing track search, mainly due to the small ratio S/B.